Single-band model for diluted magnetic semiconductors: Dynamical and transport properties and relevance of clustered states

G. Alvarez and E. Dagotto
National High Magnetic Field Lab and Department of Physics, Florida State University, Tallahassee, Florida 32310, USA
(Received 18 March 2003; published 29 July 2003)

Dynamical and transport properties of a simple single-band spin-fermion lattice model for (III,Mn)V diluted magnetic semiconductors (DMS's) is here discussed using Monte Carlo simulations. This effort is a continuation of previous work [G. Alvarez *et al.*, Phys. Rev. Lett. **89**, 277202 (2002)] where the static properties of the model were studied. The present results support the view that the relevant regime of J/t (standard notation) is that of intermediate coupling, where carriers are only partially trapped near Mn spins, and locally ordered regions (clusters) are present above the Curie temperature T_C. This conclusion is based on the calculation of the resistivity vs temperature, that shows a soft metal-to-insulator transition near T_C, as well on the analysis of the density-of-states and optical conductivity. In addition, in the clustered regime a large magnetoresistance is observed in simulations. Formal analogies between DMS's and manganites are also discussed.

DOI: 10.1103/PhysRevB.68.045202 PACS number(s): 75.50.Pp, 75.10.Lp, 75.30.Hx

I. INTRODUCTION

Diluted magnetic semiconductors (DMS's) are attracting much attention lately due to their potential for device applications in the growing field of spintronics. In particular, a large number of DMS studies have focused on III-V compounds where Mn doping in InAs and GaAs has been achieved using molecular beam epitaxy (MBE) techniques. The main result of recent experimental efforts is the discovery[1–4] of ferromagnetism at a Curie temperature $T_C \sim 110$ K in $Ga_{1-x}Mn_xAs$, with Mn concentrations x up to 10%. It is widely believed that this ferromagnetism is ''carried induced,'' with holes donated by Mn ions mediating a ferromagnetic interaction between the randomly localized Mn^{2+} spins. In practice, antisite defects reduce the number of holes n from its ideal value $n=x$, leading to a ratio $p=(n/x)$ substantially smaller than 1.

Until recently, theoretical descriptions of DMS materials could be roughly classified in two categories. On one hand, the multiband nature of the problem is emphasized as a crucial aspect to quantitatively understand these materials.[5–8] In this context the lattice does not play a key role and a continuum formulation is sufficient. The influence of disorder is considered on average. On the other hand, formulations based on the possible strong localization of carriers at the Mn-spin sites have also been proposed.[9,10] In this context a single impurity-band description is considered sufficient for these materials. Still within the single-band framework, but with carrier hopping not restricted to the Mn locations, recent approaches to the problem have used dynamical mean-field[11,12] or reduced-basis[13] approximations. An effective Hamiltonian for $Ga_{1-x}Mn_xAs$ was derived in the dilute limit and studied in Ref. 14. All these calculations are important in our collective effort to understand DMS materials.

However, it is desirable to obtain a more general view of the problem of ferromagnetism induced by a diluted set of spins and holes. To reach this goal it would be better to use techniques that do not rely on mean-field approximations and, in addition, select a model that has both the continuum and impurity-band formulations as limiting cases. Such an approach would provide information on potential procedures to further enhance T_C and clarify the role of the many parameters in the problem. In addition, these general considerations will be useful beyond the specific details of $Ga_{1-x}Mn_xAs$, allowing us to reach conclusions for other DMS's. An effort in this direction was recently initiated by Mayr and two of the authors.[15] A detailed Monte Carlo study of a simple model for DMS already allowed us to argue that T_C could be further enhanced—perhaps even to room temperature—by further increasing x and p from current values in DMS samples. These predictions seem in agreement with recent experimental developments since very recently $Ga_{1-x}Mn_xAs$ samples with T_C as high as 150 K were prepared,[16] a result believed to be caused by an enhanced free-hole density. Also samples with $T_C \sim 127$ K and $x > 0.08$ were reported in Ref. 17, and, very recently, a T_C of 140 K was achieved on high quality GaMnAs films grown with arsenic dimers.[18] There seems to be plenty of room to further increase the critical temperatures according to these theoretical calculations.

The model used in Ref. 15 was a single-band lattice Hamiltonian, also studied by other groups, which does not have the multiband characteristics and spin-orbit couplings of the real problem. However, it contains spin and holes in interaction and it is expected to capture the main qualitative aspects of carrier-induced ferromagnetism in DMS materials. The choice of a single-band model allows us to focus on the essential aspects of the problem, leaving aside the numerical complexity of the multiband Hamiltonian, which unfortunately cannot be studied with reliable numerical techniques at present without introducing further approximations.[19] Note that a quite similar philosophy has been followed in the related area of manganites for many years. In fact, it is well known that the orbital order present in those compounds can only be studied with a two-band model. However, single-band approaches are sufficient to investigate the competition between ferromagnetic and antiferromagnetic states, an effect recently argued to be at the heart of the colossal magne-

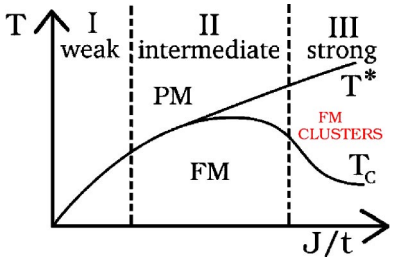

FIG. 1. Phase diagram of the single-band model Eq. (1), as discussed in Ref. 15. The figure shows schematically the three coupling regions discussed in the text: (I) weak, (II) intermediate, and (III) strong coupling, as well as the T_C and T^* dependence on the coupling J/t. The region between T^* and T_C contains FM ''clusters,'' with magnetic moments that are not aligned.

toresistance phenomenon.[20,21] As a consequence, a qualitatively reliable study of the single-band DMS model—with itinerant holes and localized classical spins—is expected to be important for progress in the DMS context as well.

In our previous publication[15] the phase diagram of the single-band model for DMS's was already sketched.[22] This phase diagram is reproduced in Fig. 1. The only parameter in the Hamiltonian is the ratio J/t, where J is the local antiferromagnetic coupling between the spins of carriers and localized Mn^{2+} ions, and t is the carrier-hopping amplitude (for details, see the full form of the Hamiltonian in the next section). Due to its large value 5/2, the Mn spin is assumed to be classical for numerical simplicity. At small J/t, individual carriers are only weakly bounded to the Mn spins. Even for small realistic values of x, the carrier wave functions strongly overlap and a large-bandwidth itinerant band dominates the physics. In this regime, T_C grows with J/t. This portion of the phase diagram is referred to as ''weak coupling'' in Fig. 1, and in our opinion it qualitatively corresponds to the continuum-limit approach pursued in Refs. 5–7. In the other extreme of large J/t, the previous effort[15] found a T_C that is much suppressed, converging to zero as J/t increases (at least at small values of x). The reason for this behavior is the strong localization of carriers at Mn spin locations, to take advantage of the strong J coupling. The localization suppresses the mobility and the carrier-induced mechanism is no longer operative. However, when several Mn spins are close to one another small regions can be magnetized efficiently. As a consequence, a picture emerges where small islands of ferromagnetism are produced at a fairly large temperature scale T^* ($>T_C$) that grows with J, but a global ferromagnetic state is only achieved upon further reducing the temperature such that the overlaps of wave functions induce a percolationlike process that aligns the individual preformed clusters. The proper procedure to distinguish between these two regimes is through an analysis of short- and long-distance spin correlations. In our opinion, the effort of Refs. 9 and 10 belongs to this class, and it corresponds to the ''strong coupling'' region of Fig. 1. Between the weak- and strong-coupling domains, an *intermediate region* provides a natural interpolation between those two extreme cases. The Curie temperature is optimal (i.e., the largest) in this intermediate zone, at fixed values of p and x. In this regime, there is sufficient interaction between the clusters to become globally ferromagnetic, and at the same time the J is sufficiently strong to induce a robust T_C. If chemical control over J/t were possible, this intermediate region would be the most promising to increase the Curie temperature (again, at fixed x and p).

However, it may even occur that the DMS materials are already in the intermediate optimal range of J/t couplings. An indirect way to test this hypothesis relies on calculations of dynamical and transport properties, which are presented in this paper, and its comparison with experiments. In particular, the experimentally measured dc resistivity ρ_{dc} of DMS compounds has a nontrivial shape with a (poor) metallic ($d\rho_{dc}/dT>0$) behavior below T_C, which turns to insulating ($d\rho_{dc}/dT<0$) at higher temperatures. This nontrivial profile resembles results reported in the area of manganites, which also have a metal-insulator transition as a function of temperature,[21] although in those materials the changes in resistivity with temperature are far more dramatic than in DMS. The formal similarities DMS manganites have already been remarked in previous literature,[15] and suggest a common origin of the ρ_{dc} vs temperature curves. In Mn oxides it is believed that above the Curie temperature, preformed ferromagnetic clusters with random orientations contribute to the insulating behavior of those materials.[20,21] For DMS's, a similar rationalization can be envisioned if the state of relevance above T_C has preformed magnetic clusters. From the previous discussion[15] it is known that the intermediate J/t region can have clusters without collapsing T_C to a very small value. At the Curie temperature, the alignment of these preformed moments leads to a metallic state. An explicit calculation of the resistivity—using techniques borrowed from the mesoscopic physics context—is provided in this paper, and the results support the conjecture that clustered states can explain the transport properties of DMS's. These unveiled analogies with manganites are not just accidental. Clearly, approaches to DMS's that rely on mobile carriers and localized spins in interaction have close similarities with the standard single-band double-exchange model where only one e_g orbital is considered. The key difference is the presence of strong dilution in DMS's as compared with manganites.

It is interesting to remark that in agreement with the ''clustered'' state described here, recently Timm and von Oppen have shown that *correlated* defects in DMS's are needed to describe experimental data.[23] Their simulations with Coulombic effects incorporated lead to cluster formation, with sizes well beyond those obtained from a random distribution of Mn sites as considered here. In this respect, the results of Ref. 23 provide an even more dramatic clustered state than ours. If the Mn spins were not distributed randomly in our simulations but in a correlated manner, the state above T_C would be even more insulating than reported below and the physics would resemble much closer that observed in manganites. Note also that Kaminski and Das Sarma have also independently arrived to a polaronic state[24] that qualitatively resembles the clustered state discussed here. It is also interesting that in recent ion-implanted (Ga,Mn)P:C experiments that reported a high Curie temperature, the presence of fer-

romagnetic clusters were observed and they were attributed to disorder and the proximity to a metal-insulator transition.[25] Even directly in (Ga,Mn)As, the inverse magnetic susceptibility deviates from the Curie law at temperatures above T_C [Fig. 2(b) of Ref. 2], which may be an indication of an anomalous behavior. In manganites, these same anomalies in the susceptibility are indeed taken as evidence of the formation of clusters.[20]

The paper is organized as follows: In Sec. II the details of the method of simulation, definitions, and conventions are presented. Section III describes the results for the density of states (DOS) of this model, the appearance of an ''impurity band'' at large J/t, and the relation of the DOS with the optimal T_C. The temperature and carrier dependence of the optical conductivity and Drude weight are presented in Sec. IV, with results compared with experiments. In Sec. V, the resistance of a small cluster is calculated and also compared with experimental data. The intermediate coupling regime is the only one found to qualitatively reproduce the available resistivity vs temperature curves. From this perspective, both the weak- and strong-coupling limits are not realistic to address DMS materials. In Sec. VI, the influence of a magnetic field is studied by calculating the magnetoresistance. Large effects are observed. Section VII describes the characteristics of the clustered-state regime above T_C at strong coupling. Finally, in Sec. VIII the ''transport'' phase diagram is presented, and it is discussed in what region it appears to be the most relevant to qualitatively reproduce results for $Ga_{1-x}Mn_xAs$ MBE-grown films.

II. METHOD AND DEFINITIONS

A. Hamiltonian formalism

There are two degrees of freedom in the DMS problem described here: (i) the local magnetic moments corresponding to the five electrons in the *d* shell of each Mn impurity, with a total spin 5/2, and (ii) the itinerant carriers produced by the Mn impurities. Since these Mn impurities substitute Ga atoms in the zinc-blende structure of GaAs, there is, in principle, one hole per Mn. However, it has been found that the system is heavily compensated and, as a consequence, the actual concentration of carriers is lower. In the present study, both the density of Mn atoms x and the density of carriers n are treated as independent input parameters. Moreover, the ratio $p=n/x$ is defined, which is a measure of the compensation of the system, e.g., for $p=0$ the system is totally compensated and for $p=1$ there is no compensation.

The Hamiltonian of the system in the one-band approximation can be written as

$$\hat{H}=-t\sum_{\langle ij\rangle,\sigma}\hat{c}^{\dagger}_{i\sigma}\hat{c}_{j\sigma}+J\sum_{I}\vec{S}_I\cdot\vec{\sigma}_I, \tag{1}$$

where $\hat{c}^{\dagger}_{i\sigma}$ creates a carrier at site i with spin σ. The carrier-spin operator interacting antiferromagnetically with the localized Mn spin $\vec{S}_I$ is $\vec{\sigma}_I=\hat{c}^{\dagger}_{I\alpha}\vec{\sigma}_{\alpha,\beta}\hat{c}_{I\beta}$. Through nearest-neighbor hopping, the carriers can hop to *any* site of the square or cubic lattice. The interaction term is restricted to a randomly selected but fixed set of sites, denoted by I. Note that in addition to the use of a single band, there are other approximation in the model described here: (i) The Hubbard U/t is not included. This is justified based on the low-carrier concentration of the problem, since in this case the probability of double occupancy is small. In addition, Mn-oxide investigations[20,21] have shown that an intermediate or large J coupling acts similarly as U/t, also suppressing double occupancy. (ii) A nearest-neighbors antiferromagnetic coupling between the Mn spins is not included. Again, this is justified as long as x is small. (iii) Finally, also potential disorder is neglected (together with the spin, the Mn sites should in principle act as charge trapping centers). This approximation is not problematic when the Fermi energy is larger than the width of the disorder potential (i.e., large p and x). However, in the (p, x) range analyzed in this paper it becomes more questionable to neglect this effect. Its influence will be studied in a future publication.

In the present study the carriers are considered to be electrons and the kinetic term describes a conduction band. However, in $Ga_{1-x}Mn_xAs$ the carriers are holes and the valence band has to be considered instead. Although the latter is more complicated, the simplified treatment followed here should yield similar results for both cases.[9,10,15]

The local spins are assumed to be classical which allows the parametrization of each local spin in terms of spherical coordinates: (θ_i,ϕ_i). The exact-diagonalization method for the Fermionic sector is described in this section, following Ref. 20. The partition function can be written as

$$Z=\prod_{i}^{N}\left(\int_0^{\pi}d\theta_i\sin\theta_i\int_0^{2\pi}d\phi Z_g(\{\theta_i,\phi_i\})\right), \tag{2}$$

where $Z_g(\{\theta_i,\phi_i\})=\mathrm{Tr}(e^{-\beta\hat{K}})$ is the partition function of the Fermionic sector, $\hat{K}=\hat{H}-\mu\hat{N}$, $\hat{N}$ is the number operator, and μ is the chemical potential.

In the following, a hypercubic lattice of dimension D, length L, and number of sites $N=L^D$ will be considered. Since $\hat{K}$ is a Hermitian operator, it can be represented in terms of a Hermitian matrix which can be diagonalized by an unitary matrix U such that

$$U^{\dagger}KU=\begin{pmatrix}\epsilon_1 & 0 & \dots & 0\\ 0 & \epsilon_2 & \dots & 0\\ \vdots & \vdots & \ddots & \vdots\\ 0 & 0 & \dots & \epsilon_{2N}\end{pmatrix}. \tag{3}$$

The basis in which the matrix K is diagonal is given by the eigenvectors $u_1^{\dagger}|0\rangle,\dots,u_{2N}^{\dagger}|0\rangle$, where the Fermionic operators used in this basis are obtained from the original operators through $u_m=\Sigma_{j\sigma}U^{\dagger}_{m,j\sigma}c_{j\sigma}$, with m running from 1 to $2N$.

Defining $u_m^{\dagger}u_m=\hat{n}_m$ and denoting by n_m the eigenvalues of $\hat{n}_m$, the trace can be written

$$\mathrm{Tr}_g(e^{-\beta\hat{K}})=\sum_{n_1,\dots,n_{2N}}\langle n_1\cdots n_{2N}|e^{-\beta\hat{K}}|n_1\cdots n_{2N}\rangle$$

$$= \sum_{n_1,\ldots,n_{2N}} \langle n_1 \cdots n_{2N}| e^{-\beta \sum_{\lambda=1}^{2N} \epsilon_\lambda n_\lambda} |n_1 \cdots n_{2N}\rangle, \quad (4)$$

since in the $\{u_m^\dagger|0\rangle\}$ basis, the operator $\hat{K}$ is $\Sigma_\lambda \epsilon_\lambda \hat{n}_\lambda$, and the number operator can be replaced by its eigenvalues. Thus Eq. (2) can be rewritten as

$$Z = \prod_i^N \left(\int_0^\pi d\theta_i \sin\theta_i \int_0^{2\pi} d\phi_i \right) \prod_{\lambda=1}^{2N} (1 + e^{-\beta\epsilon_\lambda}), \quad (5)$$

which is the formula used in the simulations.

B. Monte Carlo method

The integral over the angular variables in Eq. (5) can be performed using a classical Monte Carlo simulation.[26] The eigenvalues must be obtained for each classical spin configuration using library subroutines. Finding the eigenvalues is the most time consuming part of the numerical simulation. The integrand is clearly positive. Thus ''sign problems,'' in which the integrand of the multiple integral under consideration can be nonpositive, are fortunately not present in our study.

Although the formalism is in the grand-canonical ensemble, the chemical potential was adjusted to give the desired carrier density n. To do so, the equation $n(\mu) - n = 0$ was solved for μ at every Monte Carlo step by using the Newton-Raphson method.[27] This technique proved very efficient in adjusting with precision the desired electronic density and, as a consequence, our analysis can be considered as in the canonical ensemble as well, with a fixed number of carriers.

Usually, 2000–5000 Monte Carlo iterations were used to let the system thermalize, and then 5000–10 000 additional steps were carried out to calculate observables, measuring every five of these steps to reduce autocorrelations.

Since for fixed parameters there are many possibilities for the random location of Mn impurities, results are averaged over several of these disorder configurations. Approximately 10–20 disorder configurations were generally used for small lattices (4^3 and 10×10) and 4–8 for larger lattices (6^3 and 12×12). The inevitable uncertainties arising from the use of a small number of disorder configuration does not seem to affect in any dramatic way our conclusions below. This is deduced from the analysis of results for individual disorder samples. The qualitative trends emphasized in the present paper are present in all of these configurations.

C. Observables

Quantities that depend on the Mn degrees of freedom (θ_i and ϕ_i in the previous formalism) are calculated simply by averaging over the Monte Carlo configurations. Note that any observable that does not have the continuous symmetry of the Hamiltonian will vanish over very long runs. Thus it is standard in this context to calculate the absolute value of the magnetization, $|M| = \sqrt{\Sigma_{ij} \vec{S}_i \cdot \vec{S}_j}$, as opposed to the magnetization vector. Another useful quantity is the spin-spin correlation, defined by

$$C(x) = \frac{1}{N(x)} \sum_y \vec{S}_{y+x} \cdot \vec{S}_y, \quad (6)$$

where $N(x)$ is the number of nonzero terms in the sum. The correlation at a distance d is averaged over all lattice points that are separated by that distance, but since the system is diluted, the quantity must be normalized to the number of pairs of spins separated by d, to compare the results for different distances.

The observables that directly depend on the electronic degrees of freedom can be expressed in terms of the eigenvalues and eigenvectors of the Hamiltonian matrix $\hat{K}$. The DOS, $N(\omega)$, is simply given by $\Sigma_\lambda \delta(\omega - \epsilon_\lambda)$. However, the majority and minority DOS, $N_\uparrow(\omega)$ and $N_\downarrow(\omega)$, were also calculated in this study. $N_\uparrow(\omega)$ indicates the component that aligns with the local spin, i.e., $N_\uparrow(\omega)$ is the Fourier transform of $\Sigma_i \langle \tilde{c}_{i\uparrow}^\dagger(t) \tilde{c}_{i\uparrow}(0)\rangle$, where $\tilde{c}_{i\uparrow} = \cos(\theta_i/2) c_{i\uparrow} + \sin(\theta_i/2) e^{-i\phi_i} c_{i\downarrow}$. Then

$$N_\uparrow(\omega) = \sum_\lambda^{2N} \delta(\omega - \epsilon_\lambda) \Big(\sum_i^N U_{i\uparrow,\lambda}^\dagger U_{\lambda,i\uparrow} \cos^2(\theta_i/2) + U_{i\downarrow,\lambda}^\dagger U_{\lambda,i\downarrow} \sin^2(\theta_i/2) + [U_{i\uparrow,\lambda}^\dagger U_{\lambda,i\downarrow} \exp(-i\phi_i) + U_{i\downarrow,\lambda}^\dagger U_{\lambda,i\uparrow} \exp(i\phi_i)] \cos(\theta_i/2) \sin(\theta_i/2) \Big), \quad (7)$$

where for sites i without an impurity $\theta_i = \phi_i = 0$ is assumed. A similar expression is valid for $N_\downarrow(\omega)$. The optical conductivity was calculated as

$$\sigma(\omega) = \frac{\pi(1 - e^{-\beta\omega})}{\omega N} \int_{-\infty}^{+\infty} \frac{dt}{2\pi} e^{i\omega t} \langle \vec{j}_x(t) \cdot \vec{j}_x(0)\rangle, \quad (8)$$

where the current operator is

$$\vec{j}_x = ite \sum_{j\sigma} (c_{j+\hat{x},\sigma}^\dagger c_{j,\sigma} - \text{H.c.}), \quad (9)$$

with $\hat{x}$ the unit vector along the x direction. For $\omega \neq 0$, $\sigma(\omega)$ can be written as

$$\sigma(\omega) = \sum_{\lambda \neq \lambda'} \frac{\pi t^2 e^2 (1 - e^{-\beta\omega})}{\omega N} \times \frac{\left| \sum_{j\sigma} (U_{j+\hat{x}\sigma,\lambda}^\dagger U_{j\sigma,\lambda'} - U_{j\sigma,\lambda}^\dagger U_{j+\hat{x}\sigma,\lambda'}) \right|^2}{(1 + e^{\beta(\rho_\lambda - \mu)})(1 + e^{-\beta(\rho_{\lambda'} - \mu)})} \quad (10)$$

$$\times \delta(\omega + \rho_\lambda - \rho_{\lambda'}). \quad (11)$$

Both $N(\omega)$ and $\sigma(\omega)$ were broadened using a Lorentzian function as a substitute to the δ functions that appear in Eqs. (7) and (11). The width of the Lorentzian used was $\epsilon = 0.05$ in units of the hopping t.

The optical conductivity in d dimensions obeys the sum rule:

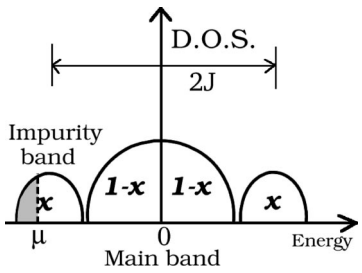

FIG. 2. Schematic representation of the DOS, for a ferromagnetic configuration and strong enough J/t coupling. The impurity band has weight x, and the chemical potential μ lies within it.

$$\frac{D}{2}=\frac{\pi e^2\langle -\hat{T}\rangle}{2Nd}-\int_{0^+}^{\infty}\sigma(\omega)d\omega, \tag{12}$$

where D is the Drude weight and $\hat{T}$ is the kinetic energy:

$$-\hat{T}=t\sum_{\langle ij\rangle,\sigma}(c_{i\sigma}^{\dagger}c_{j\sigma}+\text{H.c.}). \tag{13}$$

Although the Drude weight gives a measure of the dc conductivity properties of the cluster, the ''mesoscopic'' conductance was also calculated in order to gather additional information. The details are explained in Sec. V.

III. DENSITY OF STATES

In this section, the density of states calculated at several couplings is shown and discussed. A few basic facts about the DOS of the model, Eq. (1), are presented first. If carrier localization effects are not taken into account and a ferromagnetic state is considered at strong J/t coupling, then two spin-split bands (''impurity bands'') will appear for this model, each with weight proportional to x, at each side of the unperturbed band which would have weight $2(1-x)$ (Fig. 2). For partially compensated samples, $p<x$, the chemical potential will be located somewhere in the first spin-split band, and, as a consequence, only this band would be relevant in the model Eq. (1).

In practice, Monte Carlo simulations show that, in the regime of interest where T_C is optimal, the impurity band is not completely separated from the unperturbed band. For this reason, both the unperturbed band and the impurity band have to be considered in quantitative calculations. To illustrate this, Fig. 3 shows $N(\omega)$ vs ω for different J/t's in two dimensions. With growing J/t, the impurity band begins to form for $J/t\geqslant 3.0$, and at $J/t=6.0$ it is already fairly separated from the main band. However, note that for this extreme regime of J/t, T_C is far lower than for $J/t=3.0$, as discussed before in Ref. 15. In fact, the optimal J/t for the (x,p) parameters used here was found to be in the range 2.0–4.0. This implies that the model shows the highest T_C when the impurity band is about to form, but it is not yet separated from the main band. This introduces an important difference between our approach to DMS materials, and the theoretical calculations presented in Ref. 9. Figures 4(a)–(c) indicate that a similar behavior is found in three dimensions. In this case, once again, the optimal T_C occurs for intermediate J/t, as seen in Fig. 4(d) where the phase diagram obtained from a 6^3 lattice with $x=0.25$ and $p=0.3$ is shown.

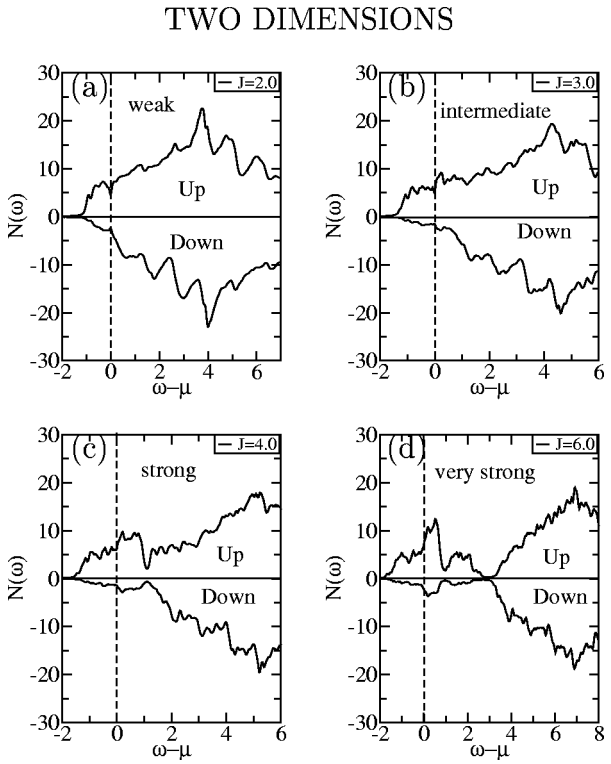

FIG. 3. $N_{\uparrow}(\omega)$ and $N_{\downarrow}(\omega)$ vs $\omega-\mu$ for a 10×10 periodic system with 26 spins ($x\sim 0.25$) and 10 electrons ($p\sim 0.4$) at $T/t=0.01$. Results are shown for (a) $J/t=2.0$, (b) $J/t=3.0$, (c) $J/t=4.0$, and (d) $J/t=6.0$. $\omega-\mu$ is in units of the hopping t. The results are averages over eight configurations of disorder (but there is no qualitative difference in the results from different configurations).

The physical reason for this behavior is that at very large J/t, the states of the impurity band are highly localized where the Mn spins are. Local ferromagnetism can be easily formed, but global ferromagnetism is suppressed by the concomitant weak coupling between magnetized clusters.

Both Figs. 3 and 4 represent results obtained at particular values of parameters $x=0.25$, $p=0.3$, and $T/t=0.01$. However, results for several other sets $\{(x,p,T)\}$ were gathered as well (not shown). The x dependence of the DOS is simple: increasing x produces a proportional increase in the number of states of the impurity band, and a corresponding decrease of the main band weight (see Fig. 2). In terms of p, increasing the effective carrier concentration by a small amount was found to simply shift the chemical potential to the right. Concerning the temperature dependence of the DOS, at low temperature the states contributing to the impurity band are polarized, i.e., the system is ferromagnetic (FM), as shown by the different weights of the majority and minority bands (Figs. 3 and 4). As the temperature increases, spin disorder grows due to thermal fluctuations, and when $T\sim T^*$, i.e., in the paramagnetic regime, the bands become symmetric.

It appears that the only change that a small increase in the carrier concentration produces is an increase in the chemical potential. However, experimentally the appearance of a

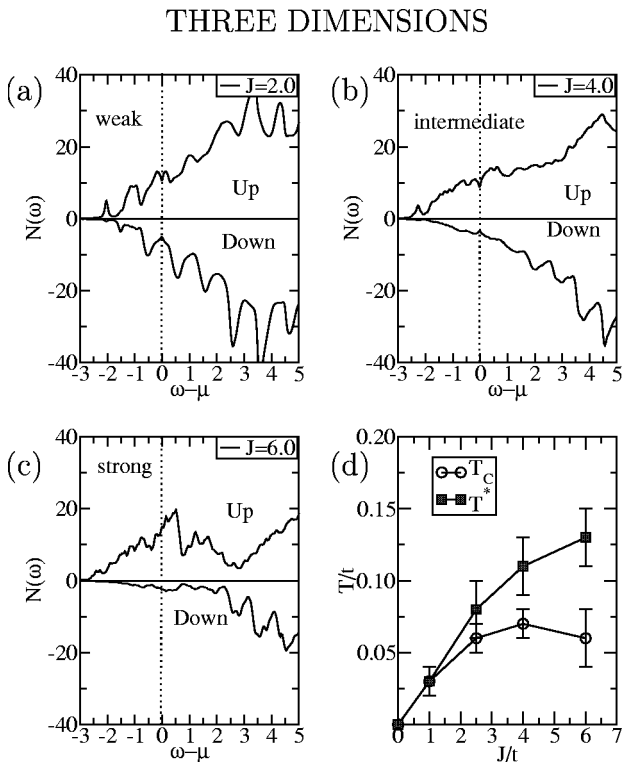

FIG. 4. $N_{\uparrow}(\omega)$ and $N_{\downarrow}(\omega)$ vs $\omega-\mu$ for a 6^3 periodic system with 54 spins ($x\sim 0.25$) and 16 electrons ($p\sim 0.4$) at $T/t=0.01$. Results are shown for (a) $J/t=2.0$, (b) $J/t=4.0$, (c) $J/t=6.0$. $\omega-\mu$ is in units of the hopping t. The results are averages over eight configurations of disorder (but there is no qualitative difference in the results from different configurations). (d) T_C and T^* vs J/t for a 6^3 lattice with $x=0.25$ and $p=0.4$. These temperatures were determined from the spin-spin correlations at short and large distances, as explained in Ref. 15.

pseudogap at the Fermi energy has been reported.[29] Although the finite-size effects in the present theoretical calculation do not allow for a detailed study of $N(\omega)$ at or very near the Fermi energy with high enough precision, in certain cases a pseudogap was indeed observed in the present study at the chemical potential, particularly when the system is in the clustered regime. While this result certainly needs confirmation, it is tempting to draw analogies with the more detailed calculations carried out in the context of manganites, where the presence of a pseudogap both in theoretical models and in experiments is well established.[20,21,30] Pseudogaps are also present in underdoped high-temperature superconductors. Given the analogies between DMS materials and transition-metal oxides unveiled in previous investigations,[15] it would not be surprising that DMS presents a pseudogap in the clustered regime as well. More work is needed to confirm these speculations.

Results presented in this section for the DOS qualitatively agree with those found in Ref. 12 using the dynamical mean-field technique (DMFT) in the coupling regime studied there. However, the DMFT approach is a mean-field approximation local in space and, as a consequence, the state emphasized in this paper—with randomly distributed clusters—cannot be studied accurately with such a technique.

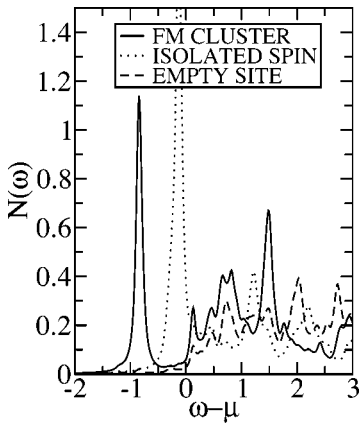

FIG. 5. Local DOS for three different classes of sites (see text) on an 8×8 lattice with $J/t=2.5$, $T/t=0.01$, $x\sim 0.2$, and $p=0.4$. This coupling regime corresponds to the intermediate optimal region, where the impurity band is not fully formed. "FM CLUSTER" is $N_{\rm I}(\omega)$ in the text notation, while "ISOLATED SPIN" and "EMPTY SITE" are $N_{\rm II}(\omega)$ and $N_{\rm III}(\omega)$, respectively.

Experimental evidence of the formation of the impurity band for $Ga_{1-x}Mn_xAs$ has been provided by Okabayashi *et al.* in Refs. 31 and 32 (see also Ref. 33). It is interesting to remark that half the total width of the impurity band obtained in our simulations is about $2t$ (see, e.g., Figs. 3 and 4), and using $t=0.3$ eV,[15] this is equal to 0.6 eV, in good agreement with the width 0.5 eV estimated from the photoemission experimental measurements mentioned before.[31]

The local DOS is studied next. The purpose of this analysis is to further understand the inhomogeneous state that forms as a consequence of Mn-spin dilution and concomitant carrier localization. The local DOS is shown in Fig. 5 on an 8×8 lattice at $x=0.25$, $p=0.4$, $J/t=2.5$, and $T/t=0.05$. In this particular case only, an arrangement of classical spins was introduced "by hand" such that the clusters are clearly formed. In this way, sites can easily be classified in three groups, as discussed below. Despite using a particularly chosen spin configuration, the resulting DOS is similar to those obtained previously (Fig. 3) using a truly random distribution of spins. Lattice sites are classified as follows: the first group is defined to contain lattice sites that have a classical spin and belong to a spin cluster. The second class is composed of sites that have an isolated classical spin, i.e., nearby sites do not have other classical spins. Finally, lattice sites without classical spins in the same site or its vicinity belong to the third class. $N_{\rm I}(\omega)$, $N_{\rm II}(\omega)$, and $N_{\rm III}(\omega)$ denote the local DOS at sites corresponding to each of the three classes, respectively. It can be observed that $N_{\rm I}(\omega)$ contributes to states inside the impurity band (note the sharp peak near -1), but also contributes to the main band since the J/t used is intermediate. $N_{\rm II}(\omega)$ contributes a sharp peak near zero, and also has weight in the main band. This can be explained as follows: the electron is weakly localized at an isolated site yielding a state at $\omega_{\rm II}\approx -J$ or, since $\mu\approx -J$ for $p\approx 0.4$, $\omega_{\rm II}-\mu\approx 0$ [see Fig. 5(a)]. This interesting result shows that many of the states near zero in Figs. 3 and 4 may be *localized*, and they do not contribute to the conductivity. Finally, in $N_{\rm III}(\omega)$ the empty sites contribute weight only in nearly

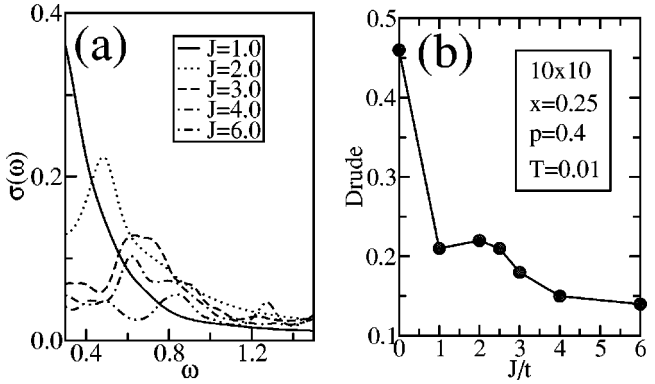

FIG. 6. Coupling dependence of the conductivity at low temperature in two dimensions. (a) $\sigma(\omega)$ vs ω for a 10×10 periodic system with 26 spins ($x\sim0.25$), 10 electrons ($p\sim0.4$), $T/t=0.01$, and for different J/t's as shown. (b) Drude weight D vs J/t for the same lattice and parameters as in (a).

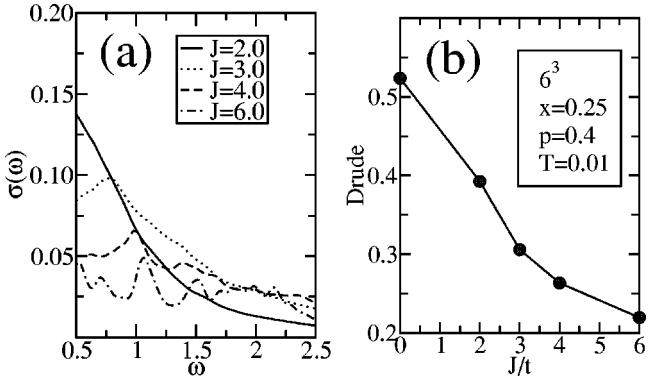

FIG. 7. Coupling dependence of the conductivity at low temperature in three dimensions. (a) $\sigma(\omega)$ vs ω for a 6^3 periodic system with 54 spins ($x\sim0.25$), 16 electrons ($p\sim0.4$), $T/t=0.01$, and for different J/t's as shown. (b) D vs J/t for the same lattice and parameters as in (a).

unperturbed states, i.e., states that belong to the main band. In conclusion, the local carrier density is very inhomogeneous and this fact has an important effect on the form of the site-integrated DOS. Our results show that scanning tunneling microscopy (STM) experiments would be able to reveal the clustered structure proposed here, if it indeed exists, when applied to DMS materials.

IV. OPTICAL CONDUCTIVITY

In the previous section, it was argued that at the optimal coupling $J/t-$ where T_C is maximized—the impurity band is not completely separated from the main band. This conclusion is supported by results obtained from the optical conductivity as well, which is shown in Fig. 6(a) for a two-dimensional lattice. This optical conductivity has two main features: (i) a zero-frequency or Drude peak and (ii) a finite-frequency broad peak which is believed to correspond to transitions from the impurity band to the main band, as argued below. From Fig. 6(a), it is observed that interband transitions are not much relevant at weak coupling ($J/t=1.0$), but they appear with more weight at intermediate couplings ($J/t=2.0$–3.0), where T_C is optimal. It is worth remarking that at J/t strong enough, e.g., $J/t=6.0$, when the impurity band is well formed, the finite-frequency peak is weaker in strength than for the optimal J/t due to localization. In fact, if J/t were so large that the impurity band is completely separated from the unperturbed band, then carrier localization would be so strong that interband transitions would not be possible. The Drude peak is plotted separately in Fig. 6(b) as a function of J/t at low temperatures. As expected, when J/t increases and localization sets in, the conductivity of the cluster decreases. Similar results for the optical conductivity and Drude weight are found in three dimensions (see Fig. 7).

The rise in absorption that appears for $J/t\geqslant2.5$ at intermediate frequencies is due to interband transitions, i.e., transitions from the impurity band to the unperturbed band. The frequency of this peak, ω_{inter}, depends upon J/t as well as carrier concentration p, but for $J/t\geqslant2.5$ (which is an intermediate value) and $p=0.4$ (a realistic value), it was observed that $0.5t\leqslant\omega_{inter}\leqslant1.0t$. The model parameter t was previously estimated[15] to be $t\sim0.3$ eV, yielding 0.15 eV$\leqslant\omega_{inter}\leqslant0.3$ eV, in agreement with experiments (see below).

The temperature dependence of $\sigma(\omega)$ is shown in Fig. 8, and it is as follows: for $T\leqslant T_C$, the Drude weight D decreases in intensity as temperature increases and the same behavior is observed for the finite-frequency peak. When $T\geqslant T_C$, D increases slightly at first and then remains constant as the temperature is increased further. This slight raise in D is subtle and could be linked to the decrease in resistivity observed for $T>T_C$ for intermediate J/t as explained in the next section, since the system is clustered just above T_C. Since both the optical conductivity and Drude weight decrease with temperature, to satisfy the sum rule the kinetic energy must also decrease as temperature increases. This is indeed observed (not shown) and is to be expected since localization of the wave function is stronger above T_C.

A broad peak at around 0.2 eV is experimentally observed in the optical conductivity of $Ga_{1-x}Mn_xAs$, as shown in Fig. 9 which is reproduced from Ref. 3. This feature has been

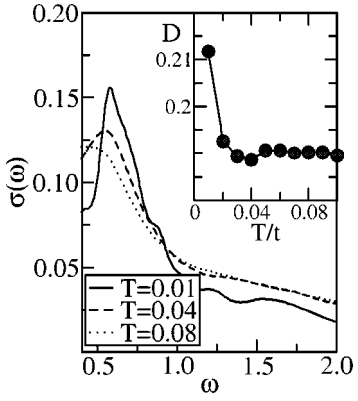

FIG. 8. Temperature dependence of the optical conductivity of model Eq. (1). Shown is $\sigma(\omega)$ vs ω for a 10×10 periodic system with 26 spins ($x\sim0.25$), $J/t=2.5$, $p=0.3$, and for different temperatures, as indicated. Inset: Drude weight D vs temperature T.

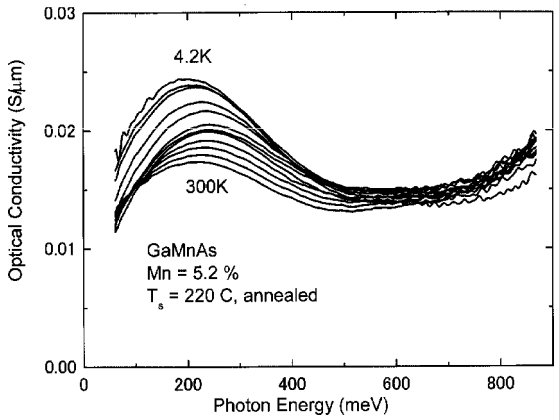

FIG. 9. Absorption coefficient $\alpha(\omega)$ spectra for a metallic sample prepared by low temperature annealing. The temperatures from down to top are 300, 250, 200, 150, 120, 100, 80, 60, 40, 20, 10, and 4.2 K (from Katsumoto *et al.*, Ref. 3).

explained before in two different ways: (i) as produced by transitions from the impurity band to the GaAs valence band[12] or (ii) as caused by intervalence band transitions.[6] Due to the frequency range and temperature behavior observed, our study supports the first possibility, i.e., that the finite-frequency peak observed for $Ga_{1-x}Mn_xAs$ at around 0.2 eV is due to transitions from the impurity band to the main band. Recent observations[34] also appear to support this view.

The Drude weight increases in intensity with increasing carrier density, as can be seen from Fig. 10. In fact, the ratio p of carriers to Mn concentration, which is a measure of the compensation of the samples, could explain, within the framework of this model, the different behavior observed at low frequencies for GaMnAs and InMnAs. In the former case, no tail of the Drude peak is found. However, for InMnAs, a clear Drude tailing is observed,[3,28] with increasing intensity as the temperature increases. At large enough doping, our calculations based on model Eq. (1) predict a Drude-like peak for $\sigma(\omega)$ which could correspond to the regime

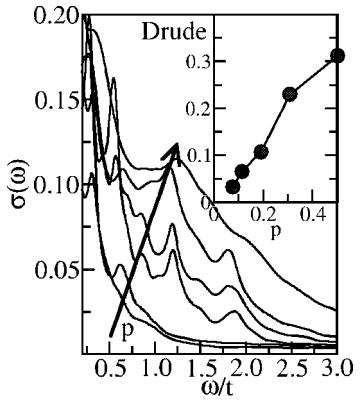

FIG. 10. p dependence of the optical conductivity. Shown is $\sigma(\omega)$, including the Drude weight, vs ω for a 10×10 lattice, $x=0.25$, $J/t=2.5$, $T/t=0.01$, and different values of p. In the direction of the arrow, p takes the values 0.08, 0.12, 0.20, 0.30, 0.38, and 0.5. Inset: Drude weight D vs fraction of carriers p.

FIG. 11. Geometry used for the calculation of the conductance. The interacting region (cluster) is connected by ideal contacts to semi-infinite ideal leads.

valid for InMnAs, while for low doping this study predicts a very small Drude peak, which is the case for GaMnAs. Unfortunately, the precise carrier concentrations for both materials are not known experimentally with precision.

V. CONDUCTANCE AND METAL-INSULATOR TRANSITION

The conductance G is calculated using the Kubo formula adapted to geometries usually employed in the context of mesoscopic systems.[35] The actual expression is

$$G=2\frac{e^2}{h}\mathrm{Tr}[(i\hbar\hat{v}_x)\mathrm{Im}\hat{\mathcal{G}}(E)(i\hbar\hat{v}_x)\mathrm{Im}\hat{\mathcal{G}}(E)], \qquad (14)$$

where $\hat{v}_x$ is the velocity operator in the x direction and $\mathrm{Im}\hat{\mathcal{G}}(E)$ is obtained from the advanced and retarded Green functions using $2i\,\mathrm{Im}\hat{\mathcal{G}}(E)=\hat{\mathcal{G}}^R(E)-\hat{\mathcal{G}}^A(E)$, where E is the Fermi energy. The cluster is considered to be connected by ideal contacts to two semi-infinite ideal leads, as represented in Fig. 11. Current is induced by an infinitesimal voltage drop. This formalism avoids some of the problems associated with finite systems, such as the fact that the conductivity is given by a sum of Dirac δ functions, since the matrix eigenvalues are discrete. A zero-frequency delta peak with finite weight corresponds to an ideal metal—having zero resistance—unless an arbitrary width is given to that delta peak. In addition, in numerical studies sometimes it occurs that the weights of the zero-frequency delta peak are negative due to size effects.[36] For these reasons, calculations of dc resistivity using finite close systems are rare in the literature. All these problems are avoided with the formulation described here.

The entire equilibrated cluster as obtained from the MC simulation is introduced in the geometry of Fig. 11. The ideal leads enter the formalism through self-energies at the left/right boundaries, as described in Ref. 35. In some cases a variant of the method explained in Ref. 35 was used in this paper to calculate the conductance (this modification was suggested to us by J. Vergés). Instead of connecting the cluster to an ideal lead with equal hoppings, a replica of the cluster was used at the sides. This method, although slightly slower, takes into account all of the Monte Carlo data for the cluster, including the periodic boundary conditions. In addition, averages over the random Mn spin distributions are carried out. The physical units of the conductance G in the numerical simulations are e^2/h as can be inferred from Eq. (14). In Fig. 12 the inverse of the conductance, which is a measure of the resistivity, is plotted for a three-dimensional lattice at weak, intermediate, and strong coupling, at fixed $x=0.25$ and $p=0.3$. For the weak-coupling regime ($J/t=1.0$) the system is weakly metallic at all temperatures. In

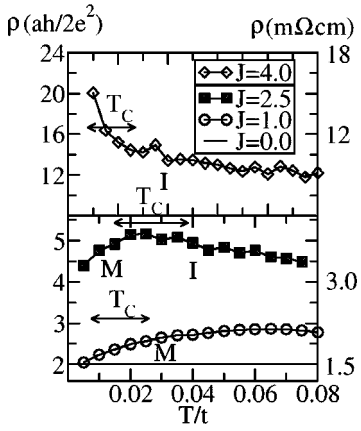

FIG. 12. Dependence of the theoretically calculated resistivity ρ with temperature in three dimensions. Shown is $\rho = L/G$ vs T on 4^3 lattices, 16 spins ($x = 0.25$), and 5 carriers ($p = 0.3$) for the J/t's indicated. An average over 20 disorder configurations has been performed in each case. Units are shown in two scales, $ah/(2e^2)$ on the left and mΩ cm on the right, with $L = 4$ and assuming $a = 5.6$ Å. The estimated critical temperatures are also shown (the arrows indicate the current accuracy of the estimations).

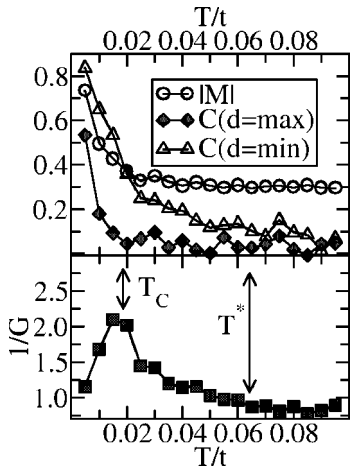

FIG. 14. Magnetization $|M|$, spin-spin correlations $C(d)$, at maximum and minimum distance, and inverse of the conductance $1/G$ vs T on a 12×12 lattice with 22 spins ($x \approx 0.15$), 6 electrons ($p \approx 0.3$), and $J/t = 1.0$. The approximate vanishing of spin correlations at different temperatures, depending on the distance d studied, allowed us to obtain an approximate determination of T_C and T^*, similarly as carried out in previous studies (Ref. 15).

the other limit of strong couplings, $1/G$ decreases with increasing temperature, indicating a clear insulating phase, as a result of the system being in a clustered state at the temperatures explored,[10,15] with carriers localized near the Mn spins. At the important intermediate couplings emphasized in our effort, the system behaves like a dirty metal for $T < T_C$, while for $T_C < T < T^*$, $1/G$ slightly decreases with increasing temperature, indicating that a soft metal to insulator transition takes place near T_C. For $T > T^*$, where the system is paramagnetic, $1/G$ is almost constant. Note that for strong enough J/t, $T_C \to 0$ and therefore no metallic phase is present.

Similar qualitative behavior is found for the two-dimensional case (Figs. 13 and 14). Furthermore, in Fig. 14 the spin-spin correlations have been plotted to show the location of T_C and T^* and their relation to the resistivity.

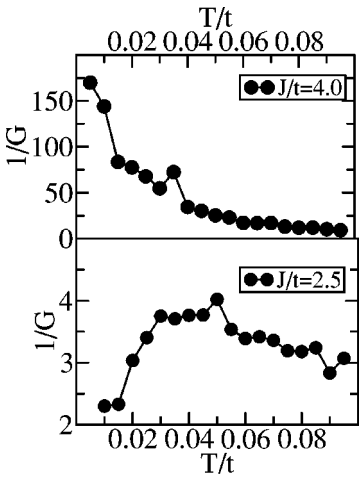

FIG. 13. Inverse of the conductance $1/G$ vs T calculated on a 10×10 lattice with 26 spins ($x \sim 0.25$), 8 electrons ($p \approx 0.3$), and 2 values of J/t as indicated. Shown is an average over three disorder configurations. $1/G$ has units of $h/(2e^2)$ in two dimensions.

It is interesting to compare our results with experiments. For $Ga_{1-x}Mn_xAs$, data similar to those found in our investigations have been reported.[2,3] A typical result for resistivity versus T can be found in Ref. 4. The qualitative behavior of the resistivity in these samples agrees well with the theoretical results presented in Fig. 12 if intermediate couplings are considered. On the other hand, stronger or weaker couplings are not useful to reproduce the data, since the result is either insulating or metallic at all temperatures, respectively (defining metallic and insulator regimes by the slope of the resistivity vs temperature curves).

Furthermore, even the experimental numerical values of the resistivity are in agreement with the results presented here [even though model Eq. (1) does not include a realistic treatment of the GaAs host bands]. This can be shown as follows. The conductivity of a three-dimensional sample is related to the conductance by $\sigma = G/L$, where L is the side length of the lattice. Hence the resistivity is $\rho = L/G$. The units of G are, as explained before, $h/(2e^2)$, and in our case $L = 4a$, where a is the lattice spacing. Assuming $a = 5.6$ Å, then the values shown in Fig. 12 are obtained. Note that in Fig. 12 the minimum resistivity for $J/t = 2.5$ is 3.3 mΩ cm, whereas the minimum possible value for that carrier doping and cluster size used is 1.5 mΩ cm, which corresponds to the case $J/t = 0$. In spite of the label ''metallic'' for these results, the absolute values of the resistivity are high. Similarly, in the metallic phase of the sample shown in the experimental results of Ref. 4, the minimum resistivity is only ~ 3–6 mΩ cm. Both in theory and experiments, the metallic phase appears to be ''dirty,'' which is likely due to the reduced number of carriers, and localizing effect of the disorder.

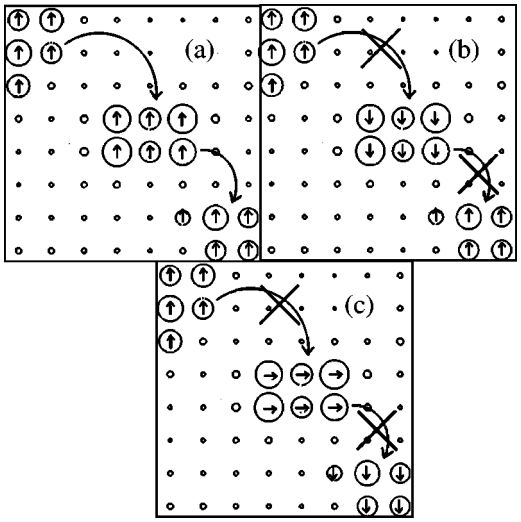

FIG. 15. Qualitative explanation of the transport properties of clustered states. Shown are three clusters created by hand on an 8×8 lattice and with spin configurations also selected by hand to illustrate our ideas. For a (a) FM state at $J/t=2.5$ and $p=0.4$, conduction is possible due to the alignment of magnetic moments and the conductance was found to be $G=2.8(2e^2/h)$. For the clustered state regime, two typical configurations (b) and (c) are shown where the conduction channels are broken and as a consequence $G\approx0$. For the same clustered state but with randomly selected spin orientations (not shown) the conductance is small but finite $G\approx0.5(2e^2/h)$. The radius of the solid circles represent the local charge density.

For J/t intermediate or strong, localization of the wave function is observed at intermediate temperatures.[15] This implies that carriers tunnel between impurity sites without visiting the main band, leading to insulating behavior. Below T_C conduction is favored by the ferromagnetic order and, as a consequence, as temperature decreases conductance increases. To further understand why the conductance (resistance) has a minimum (maximum) around T_C it is helpful to consider the three states: FM, clustered, and paramagnetic (PM) as depicted for a special spin configuration in Fig. 15 on an 8×8 lattice. This configuration is not truly random but it was chosen by hand for simplicity so that the spin clusters can easily be recognized. In the case of a random configuration of spins a similar reasoning can be drawn. For the FM state of Fig. 15, conduction is possible and indeed the measured conductance is $G\approx2.8(2e^2/h)$. For the two possible clustered states represented in Figs. 15(b) and (c), the conduction is reduced due to the different alignment of spins in different clusters. This is verified by calculating the conductance which is $G\approx0.0$ in those cases. For a paramagnetic spin arrangement with spin pointing in random directions (not shown), the conductance is small but finite, $G\approx0.5(2e^2/h)$. It follows that the clustered state has the minimum conductance, and this explains the observed behavior of the resistivity with a maximum near T_C, i.e., when the system is clustered.

The inverse of the Drude weight D^{-1} also shows a peak around T_C as seen in Fig. 16, where the same Mn-spin configuration as in Fig. 14 was used. This provides further evidence for the metal-insulator transition near T_C described here.

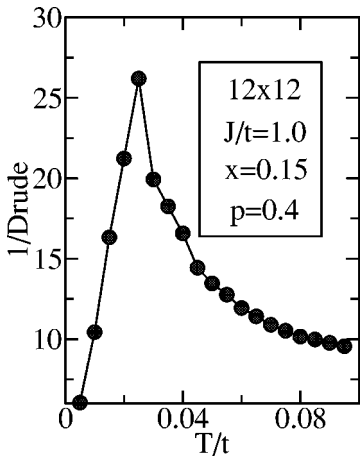

FIG. 16. Inverse of the Drude weight vs T for a 12×12 lattice and parameters as in Fig. 14. Note that both the inverse conductance in Fig. 14 and Drude^{-1} provide evidence for a metal-insulator transition at approximately the same temperature T_C.

It is also interesting to remark that the optimal value of J/t changes with x (e.g., for small x, J/t optimal is also small). Since J/t_{optimal} approximately separates the metal from the insulator, working at a fixed J/t (as in real materials) and varying x, then an insulator at high temperatures is found at small x, turning into a metal at larger x. This is in excellent agreement with the experimental results of Ref. 4 using a careful annealing procedure (while results of previous investigations with as-grown samples had found an insulator-metal-insulator transition with increasing x[2]). The issue discussed in this paragraph is visually illustrated in Fig. 17, for the benefit of the reader.

VI. MAGNETORESISTANCE

The magnetoresistance percentage ratio was calculated using the definition $MR=100\times[\rho(0)-\rho(B)]/\rho(B)$. Figure 18 shows the magnetization $|M|$ and the resistivity as a function of the applied field B on a 12×12 lattice, $x=0.15$, $p=0.4$, $J/t=1.0$, and low temperature. Note that in two di-

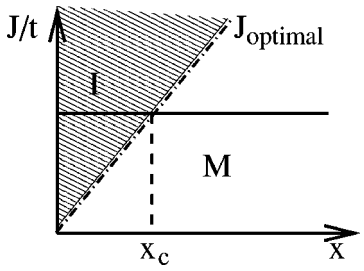

FIG. 17. Dependence of J/t_{optimal} with x, approximately separating the metal from the insulator (standard notation). At fixed J/t (horizontal solid line), as in experiments, the system should transform from an insulator to a metal with increasing x, in agreement with experiments (Ref. 4).

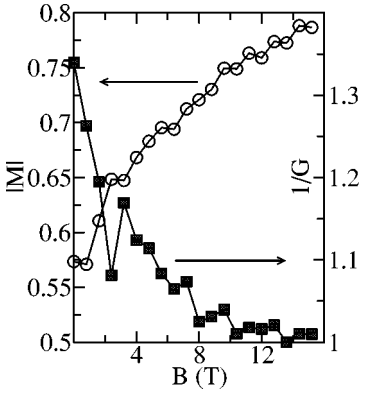

FIG. 18. Magnetization $|M|$ and inverse conductance $1/G$ vs magnetic field B on a 12×12 lattice with PBC, $x=0.15$, $p=0.3$, $J=1.0$, and $T/t=0.01$ (the same parameters as in Fig. 14). The units of B are T, assuming $g=2.0$ and $S=5/2$. The units of $1/G$ are $h/2e^2$. The approximate values of the magnetoresistance are 18% at 4 T and 30% at 12 T.

mensions at $x=0.25$ and $p=0.3$, the intermediate coupling corresponds to $J/t=2.5$, but at $x=0.15$, now $J/t=1.0$ corresponds to optimal coupling since as x decreases the optimal J/t also decreases. For these parameters, T_C was estimated to be $0.02t$ and $T^*\approx0.06t$. The value in T of the magnetic field was calculated assuming $g=2.0$ and $S=5/2$ for the localized spins. The units of the resistivity are $h/(2e^2)$ for the two-dimensional lattice.

In our simulations it was observed that $|M|$ increases with increasing magnetic field. At zero magnetic field $|M|$ is 60% of its maximum value, while at 12 T it has reached $\sim80\%$. This is in agreement with the experimental results in Fig. 3 of Ref. 2 where the magnetization is 50% of its maximum value at zero field, but it reaches 70% of that maximum value at 4 T. In our studies it was also observed that $1/G$ decreases with increasing magnetic field, showing at all fields a negative magnetoresistance. Near T_C the resistivity decreases by 20–30% increasing the field from zero to 12 T, while the decrease in resistivity at higher temperatures is much smaller. The present computational results agree very well with the experimentally measured dependence of the resistivity and magnetization on magnetic fields. For example, in Fig. 2(b) of Ref. 2, the decrease in resistivity is 25% near $T_C\approx60$ K when increasing the field from zero to 15 T. A much smaller decrease in resistivity is observed at higher temperatures ($T>120$ K). It is also indicated in that experimental reference that the magnetoresistance is between 30% and 40% at 12 T.

It is interesting to remark that substantial magnetoresistance effects have been reported in thin films consisting of nanoscale $Mn_{11}Ge_8$ ferromagnetic clusters embedded in a dilute ferromagnetic semiconductor matrix.[37] The characteristics of these materials are analogous to our clustered state, that also show a robust MR effect due to magnetization rotation of spontaneously formed clusters.

VII. MORE ABOUT CLUSTER FORMATION

It was discussed before in this paper and in previous publications that a clustered state is formed above T_C for intermediate and large J/t couplings. This state is a candidate to describe DMS materials since it explains both the resistivity maximum around T_C as well as the decrease in resistivity with increasing applied magnetic field. In addition, it provides an optimal T_C. This clustered state is formed only for intermediate or larger J/t and when the compensation is strong, $p<0.4$. Since for large J/t the carriers are localized, the problem becomes one of percolation theory, which has already been treated using different approaches and approximations.[24] Here, only a very simple way of visualizing this state will be presented. First, consider a two-dimensional lattice with 5% Mn spins represented as black dots, as shown in Fig. 19(a). The carrier wave function $\psi(r)$ is considered to be localized around a Mn spin and it is assumed to be a step function for simplicity, i.e., $\psi(r)$ is nonzero only if $r<r_l$ where r_l is the localization radius introduced by hand. Sites where the wave function is not zero are the black areas of Fig. 19(b). In this case, sites can be classified into connected regions, and that feature is indicated in Fig. 19(c) using different shades. Each region is correlated and will correspond to a FM cluster. In this case all spins belong to some large cluster. As the concentration x grows, the clusters will tend to merge. As x decreases, these clusters will become more and more isolated.

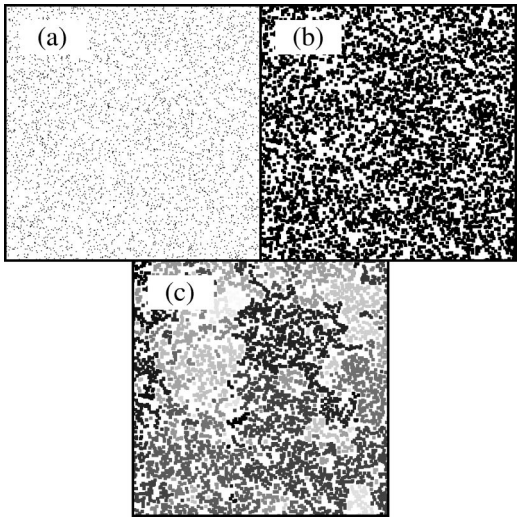

FIG. 19. Percolation picture for the formation of the clustered-state regime. (a) Two-dimensional lattice representing randomly located classical spins as black dots with $x=0.05$. (b) Black areas represent nonzero carrier wave function, assuming a step-function profile for the wave functions with radius equal to two sites, as explained in the text. (c) Same as (b) but now showing connected regions (which could in practice correspond to the FM clusters discussed in the text) indicated with different shades of gray.

Recent experimental work on (Ga,Cr)As have revealed unusual magnetic properties which were associated with the random magnetism of the alloy. The authors of Ref. 38 explained their results using a distributed magnetic polaron model that resembles the clustered-state ideas discussed here and in Refs. 15, 23, and 24.

VIII. CONCLUSIONS

In this paper, dynamical and transport properties of a single-band model for diluted magnetic semiconductors have

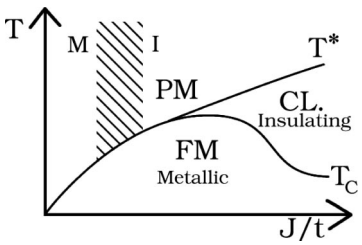

FIG. 20. Sketch of the phase diagram indicating the conducting and insulating regions, as obtained in the present investigations. The dashed area in the paramagnetic phase indicates the crossover region from a mild metallic weak-coupling regime to a mild insulating strong-coupling regime.

been presented. The calculations were carried out on a lattice and using Monte Carlo techniques. The optical conductivity, density of states, and resistance vs temperature agree with experimental data for $Ga_{1-x}Mn_xAs$ if the model is in a regime of *intermediate* J/t coupling. In this region, the carriers are neither totally localized at the Mn sites nor free, as in previous theories. The state of relevance has some characteristics of a clustered state, in the sense that upon cooling from high temperatures first small regions are locally magnetized at a temperature scale T^*−causing a mild insulating behavior—while at an even lower temperature T_C the alignment of the individual cluster moments occurs—causing metallic behavior. This is in agreement with previous investigations.[10,15,23,24]

One of the main conclusions of the paper is summarized in Fig. 20 where the ''transport'' phase diagram is sketched. The low-temperature ferromagnetic phase is metallic (although often with poor metallicity). The clustered state between T^* and T_C has insulating properties, and the same occurs in a good portion of the phase diagram above these two characteristic temperatures. Note that here the terms metallic and insulating simply refer to the slope of the resistivity vs temperature curves. The values of the resistivities in the two regimes are not very different, similarly as observed experimentally.

This and related efforts lead to a possible picture of DMS materials where the inhomogeneities play an important role. In this respect, these materials share characteristics with many other compounds such as manganites and cuprates, where current trends point toward the key importance of nanocluster formation to understand the colossal magnetoresistance and underdoped regions, respectively. ''Clustered'' states appear to form a new paradigm that is useful to understand the properties of many interesting materials.

ACKNOWLEDGMENT

The authors acknowledge the help of J. A. Vergés in the study of the conductance. The subroutines used in this context were kindly provided by him. Conversations with A. Fujimori are also gratefully acknowledged. G.A. and E.D. were supported by NSF Grant No. DMR-0122523. Additional funds have been provided by Martech (FSU). Part of the computer simulations have been carried out on the CSIT IBM SP3 system at the FSU School for Computational Science and Information Technology (CSIT).

[1] H. Ohno, Science **281**, 951 (1998); H. Ohno, J. Magn. Magn. Mater. **200**, 110 (1999).

[2] H. Ohno and F. Matsukura, Solid State Commun. **117**, 179 (2001).

[3] S. Katsumoto, T. Hayashi, Y. Hashimoto, Y. Iye, Y. Ishiwata, M. Watanabe, R. Eguchi, T. Takeuchi, Y. Harada, S. Shin, and K. Hirakawa, Mater. Sci. Eng., B **84**, 88 (2001).

[4] S.J. Potashnik, K.C. Ku, S.H. Chun, J.J. Berry, N. Samarth, and P. Schiffer, Appl. Phys. Lett. **79**, 1495 (2001).

[5] J. König, J. Schliemann, T. Jungwirth, and A.H. MacDonald, *Ferromagnetism in (III,Mn)V Semiconductors in Electronic Structure and Magnetism of Complex Materials*, edited by D.J. Singh and D.A. Papaconstantopoulos (Springer-Verlag, Berlin, 2002), and references therein.

[6] J. Sinova, T. Jungwirth, S.-R. Eric Yang, J. Kucera, and A.H. MacDonald, Phys. Rev. B **66**, 041202 (2002); S.-R. Eric Yang, J. Sinova, T. Jungwirth, Y.P. Shim, and A.H. MacDonald, Phys. Rev. B **67**, 045205 (2003); J. Sinova, T. Jungwirth, J. Kucera, and A.H. MacDonald, cond-mat/0301405 (unpublished); see also T. Jungwirth, Jürgen König, Jairo Sinova, J. Kucera, and A.H. MacDonald, Phys. Rev. B **66**, 012402 (2002).

[7] John Schliemann, Jürgen König, and A.H. MacDonald, Phys. Rev. B **64**, 165201 (2001).

[8] T. Dietl, H. Ohno, and F. Matsukura, Phys. Rev. B **63**, 195205 (2001); T. Dietl, Semicond. Sci. Technol. **17**, 377 (2002).

[9] Malcolm P. Kennett, Mona Berciu, and R.N. Bhatt, Phys. Rev. B **66**, 045207 (2002); Mona Berciu and R.N. Bhatt, Phys. Rev. Lett. **87**, 107203 (2001); see also C. Timm, F. Schäfer, and F. von Oppen, *ibid.* **90**, 029701 (2003); Mona Berciu and R.N. Bhatt, *ibid.* **90**, 029702 (2003).

[10] M. Mayr, G. Alvarez, and E. Dagotto, Phys. Rev. B **65**, 241202 (2002).

[11] A. Chattopadhyay, S. Das Sarma, and A.J. Millis, Phys. Rev. Lett. **87**, 227202 (2001).

[12] E.H. Hwang, A.J. Millis, and S. Das Sarma, Phys. Rev. B **65**, 233206 (2002).

[13] M.J. Calderon, G. Gomez-Santos, and L. Brey, Phys. Rev. B **66**, 075218 (2002).

[14] G. Zaránd and B. Jankó, Phys. Rev. Lett. **89**, 047201 (2001).

[15] G. Alvarez, M. Mayr, and E. Dagotto, Phys. Rev. Lett. **89**, 277202 (2002).

[16] K.C. Ku, S.J. Potashnik, R.F. Wang, M.J. Seong, E. Johnston-Halperin, R.C. Meyers, S.H. Chun, A. Mascarenhas, A.C. Gossard, D.D. Awschalom, P. Schiffer, and N. Samarth, Appl. Phys. Lett. **82**, 2302 (2003).

[17] I. Kuryliszyn, T. Wojtowicz, X. Liu, J.K. Furdyna, W. Dobrowolski, J.-M. Broto, M. Goiran, O. Portugall, H. Rakoto, and B. Raquet, Acta. Phys. Pol. A **102**, 659 (2002); J. Supercond. **16**, 63 (2003).

[18] R.P. Campion, K.W. Edmonds, L.X. Zhao, K.Y. Wang, C.T. Foxon, B.L. Gallagher, and C.R. Staddon, J. Cryst. Growth **251**, 311 (2003).

[19] In Ref. 7, a hybrid MC study of the multiband model for DMS was presented. In that reference the model was treated in *k* space, approximating the Fermionic trace for its zero-temperature value. On the contrary, our present work treats the Fermionic trace exactly, and calculations are performed in real space.

[20] E. Dagotto, T. Hotta, and A. Moreo, Phys. Rep. **344**, 1 (2001); see also J. Burgy, M. Mayr, V. Martin-Mayor, A. Moreo, and E. Dagotto, Phys. Rev. Lett. **87**, 277202 (2001).

[21] E. Dagotto, *Nanoscale Phase Separation and Colossal Magnetoresistance* (Springer-Verlag, Berlin, 2002).

[22] The term ''sketched'' is used instead of ''established'' due to the inevitable uncertainties of the numerical effort, which is based on nearly exact results but obtained in small clusters.

[23] C. Timm, F. Schäfer, and F. von Oppen, Phys. Rev. Lett. **89**, 137201 (2002); C. Timm and F. von Oppen, cond-mat/0209055 (unpublished).

[24] A. Kaminski and S. Das Sarma, Phys. Rev. Lett. **88**, 247202 (2002).

[25] N. Theodoropoulou, A.F. Hebard, M.E. Overberg, C.R. Abernathy, S.J. Pearton, S.N.G. Chu, and R.G. Wilson, Phys. Rev. Lett. **89**, 107203 (2002).

[26] K. Binder and D.W. Heermann, *Monte Carlo Simulations In Statistical Physics* (Springer-Verlag, Berlin, 1992).

[27] For more details, see H. Aliaga, D. Magnoux, A. Moreo, D. Poilblanc, S. Yunoki, and E. Dagotto, cond-mat/0303513 (unpublished).

[28] H. Hirakawa, A. Oiwa, and H. Munekata, Physica E (Amsterdam) **10**, 215 (2001).

[29] S.H. Chun, S.J. Potashnik, K.C. Ku, P. Schiffer, and N. Samarth, Phys. Rev. B **66**, 100408 (2002).

[30] A. Moreo, S. Yunoki, and E. Dagotto, Phys. Rev. Lett. **83**, 2773 (1999).

[31] J. Okabayashi, A. Kimura, O. Rader, T. Mizokawa, A. Fujimori, T. Hayashi, and M. Tanaka, Phys. Rev. B **64**, 125304 (2001).

[32] J. Okabayashi, T. Mizokawa, D.D. Sarma, and A. Fujimori, Phys. Rev. B **65**, 161203(R) (2002).

[33] Photoemission results for DMS materials have also been presented in H. Asklund, L. Ilver, J. Kanski, J. Sadowski, and R. Mathieu, Phys. Rev. B **66**, 115319 (2002). These experiments indicate that the Fermi energy is slightly above, but very near to, the valence-band maximum. Since in our results the Fermi energy is within the ''impurity band,'' this provides further evidence that the impurity band and the main band are not separated, but that they overlap in GaMnAs for the samples experimentally studied.

[34] E.J. Singley, R. Kawakami, D.D. Awschalom, and D.N. Basov, Phys. Rev. Lett. **89**, 097203 (2002).

[35] J.A. Verges, Comput. Phys. Commun. **118**, 71 (1999).

[36] E. Dagotto, Rev. Mod. Phys. **66**, 763 (1994), and references therein.

[37] Y.D. Park, A. Wilson, A.T. Hanbicki, J.E. Mattson, T. Ambrose, G. Spanos, and B.T. Jonker, Appl. Phys. Lett. **78**, 2739 (2001).

[38] A. Dakhama, B. Lakshmi, and D. Heiman, Phys. Rev. B **67**, 115204 (2003).